

Formation of TRAPPIST-1 and other compact systems

Chris W. Ormel, Beibei Liu, and Djoeka Schoonenberg

Anton Pannekoek Institute (API), University of Amsterdam, Science Park 904, 1090GE Amsterdam, The Netherlands
e-mail: [c.w.ormel,b.liu,d.schoonenberg]@uva.nl

April 21, 2022

ABSTRACT

TRAPPIST-1 is a nearby $0.08 M_{\odot}$ M-star, which was recently found to harbor a planetary system of at least seven Earth-mass planets, all within 0.1 au. The configuration confounds theorists as the planets are not easily explained by either *in situ* or migration models. In this Paper we present a scenario for the formation and orbital architecture of the TRAPPIST-1 system. In our model, planet formation starts at the H_2O iceline, where pebble-size particles – whose origin is the outer disk – concentrate to trigger streaming instabilities. After their formation, planetary embryos quickly mature by pebble accretion. Planet growth stalls at Earth masses, where the planet’s gravitational feedback on the disk keeps pebbles at bay. Planets are transported by Type I migration to the inner disk, where they stall at the magnetospheric cavity and end up in mean motion resonances. During disk dispersal, the cavity radius expands and the inner-most planets escape resonance. We argue that the model outlined here can also be applied to other compact systems and that the many close-in super-Earth systems are a scaled-up version of TRAPPIST-1. We also hypothesize that few close-in compact systems harbor giant planets at large distances, since they would have stopped the pebble flux from the outer disk.

Key words. planets and satellites: formation – planets and satellites: dynamical evolution and stability – planet–disc interactions – methods: analytical

1. Introduction

TRAPPIST-1 – a late-type $0.08 M_{\odot}$ M-star situated at a distance of 12 pc – is known to harbor an ultra-compact planetary system of at least six planets (Gillon et al. 2016, 2017). The seventh planet, TRAPPIST-1h, was recently confirmed by a transit timing analysis and K2 data (Luger et al. 2017). All planets are within 0.1 au of their host star. Remarkably, all planets have masses similar to Earth and the inferred densities, although highly uncertain, are consistent with rocky compositions (Gillon et al. 2017). The orbital period ratios of the TRAPPIST-1 planets indicate that planets d/e, e/f and g/h are very close to 3:2 mean motion resonance (MMR) while f/g shows a 4:3 commensurability. Planets b/c and c/d are somewhat further located from a first order MMR.

The ultra-compact configuration of the TRAPPIST-1 system raises the question how it formed. *In situ* formation, where rocky planets emerge from a giant impact phase in a gas free disks (e.g., Hansen & Murray 2012), would have required an unusually dense disk and would also not easily explain the resonant configuration. Planet migration seems to be preferred (Lee & Peale 2002). However, formation beyond the iceline cannot explain the predominantly rocky composition. In addition, traditional formation scenarios fail to explain why all planets end up at masses approximately equal to Earth’s.

In this Paper we hypothesize a different scenario: it was the planetary building blocks in the form of mm/cm-size particles (pebbles) that migrated to the inner disk. Circumstellar disks contain large amounts of pebble-size particles (e.g., Testi et al. 2014; Pérez et al. 2015); and the thermal emission from these particles has also been observed around low-mass stars or even brown dwarfs (Ricci et al. 2012). We argue that these pebbles were transformed into planetary embryos at the H_2O iceline, situated at ≈ 0.1 au, where they migrated inwards by type I migra-

tion. Interior to the H_2O iceline the planets grew by accretion of rocky pebbles. Inward planet migration ceased at the disk’s inner edge, where they migrated into first-order MMR. Later, during the disk dispersion phase, the 3:2 MMRs of the inner two planet pairs were broken, resulting in the architecture that we witness today.

The goal of this Paper is to present a synopsis of the early history of the TRAPPIST-1 system from simple analytical reasoning, which may inspire future numerical, more precise treatments. The adopted disk and stellar parameters (Table 1) have been optimized towards TRAPPIST-1 but are not out of the ordinary. In Sect. 2 we discuss the circumstellar disk of TRAPPIST-1. Section 3 presents the chronology. In Sect. 4 we speculate about the implications of our model to other stars.

2. The TRAPPIST-1 disk

2.1. Disk structure

We assume that the TRAPPIST-1 circumstellar disk can be divided in two regions:

- The inner disk, $r \ll 1$ au. This is the region where the ice-line is located, and where the planetary system forms. We further assume that the inner disk is viscously-relaxed, characterized by an α -viscosity, $\nu = \alpha h^2 r^2 \Omega$, where h , the aspect ratio, is assumed constant and $\Omega_K(r)$ the local orbital frequency. The gas surface density Σ_g follows from the accretion rate \dot{M}_g : $\Sigma_g = \dot{M}_g / 3\pi\nu$ (Lynden-Bell & Pringle 1974), where we adopt a value of $\dot{M}_g = 10^{-10} M_{\odot} \text{ yr}^{-1}$ typical for M-stars (e.g., Manara et al. 2015). The constant aspect ratio of the inner disk is motivated by viscous heating and lamp-post heating ($R_{\star}/r \sim 0.1$; Rafikov & De Colle 2006), as well

Table 1. Default disk and stellar parameters of TRAPPIST-1 during the planet formation phase .

symbol	description	value	comments
α	viscosity parameter inner disk	10^{-3}	(a)
δ_{ice}	fractional width of iceline	0.05	
γ_I	prefactor in Type-I migration rate	4	(b)
ξ	# e -foldings to reach pebble size	10	
τ_p	pebble dimensionless stopping time exterior to iceline	0.05	(c)
ζ	dust fraction in pebbles	0.5	
h	inner disk aspect ratio	0.03	
r_{out}	outer disk radius	200 au	
B_\star	stellar magnetic field strength at surface	180 G	
M_\star	stellar mass	$0.08 M_\odot$	
M_{disk}	disk mass (gas)	$0.04 M_\star$	
\dot{M}_g	accretion rate	$10^{-10} M_\odot \text{ yr}^{-1}$	
R_\star	stellar radius	$0.5 R_\odot$	
Z_0	disk metallicity (global solids-to-gas mass ratio)	0.02	

Notes. ^(a) This our default model. We also discuss more laminar and more turbulent disks ($10^{-4} \leq \alpha \leq 10^{-2}$) ; ^(b) Kley & Nelson (2012) ; ^(c) The stopping time of pebbles interior to the iceline is denoted τ_s with $\tau_s \ll \tau_p$.

as from SED-fitting (Mulders & Dominik 2012). The temperature structure corresponding to $h = 0.03$ reads:

$$T(r) = 180 \text{ K} \frac{M_\star}{0.08 M_\odot} \left(\frac{h}{0.03} \right)^2 \left(\frac{r}{0.1 \text{ au}} \right)^{-1} \quad (1)$$

- The outer disk, $r \gg 1$ au (Fig. 1). This is the region that dominates the disk mass (in solids as well as gas). Since viscous timescales ($\sim r^2/\nu$) are longer than the duration of the planet formation process (see Eq. (6)) a steady accretion disk is inappropriate. Instead, we simply adopt a power-law profile for the surface density:

$$\Sigma_{\text{g,out}} = \frac{(2-p)M_{\text{disk}}}{2\pi r_{\text{out}}^2} \left(\frac{r}{r_{\text{out}}} \right)^{-p}; \quad (p < 2) \quad (2)$$

where M_{disk} is the total disk mass and r_{out} the disk's outer radius. We choose $p = 1$, $M_{\text{disk}} = 0.04 M_\star$ and a metallicity of $Z_0 = 0.02$, which amounts to a total mass of ≈ 22 Earth masses in solids of which $\approx 11 M_\oplus$ is in rocky material (assuming a dust fraction in pebbles of $\zeta = 0.5$; Lodders 2003).

The inner disk is truncated at the magnetospheric cavity radius (e.g., Frank et al. 1992):

$$r_c = \left(\frac{B_\star^4 R_\star^{12}}{4GM_\star \dot{M}_g^2} \right)^{1/7} \approx 0.0102 \text{ au} \quad (3)$$

where B_\star is the strength of the magnetic field measured at the surface of the star (R_\star). In this and other equations the numerical value follows from inserting the default parameters listed in Table 1. Here, the surface magnetic field strength of 180 G – perhaps lower than the typical \sim kG of T-Tauri stars – is consistent with observations of brown dwarfs (Reiners et al. 2009).

In general, disks feature a negative radial pressure gradient, which causes gas to rotate slower than Keplerian by an amount ηv_K (Nakagawa et al. 1986). For our choices of $\Sigma_g(r)$ and $T(r)$ for the inner disk we obtain that $\eta = \frac{5}{4}h^2$ is constant. The sub-Keplerian motion induces the orbital decay of pebble-size particles (Weidenschilling 1977): $v_r = -2\eta v_K \tau_p / (1 + \tau_p^2) \approx -2\eta v_K \tau_p$ where $\tau_p = t_{\text{stop}} \Omega_K$, the dimensionless stopping time, is assumed less than unity. We assume that just exterior to the iceline, $\tau_p = 0.05$, a value consistent for drifting pebbles (Birnstiel et al.

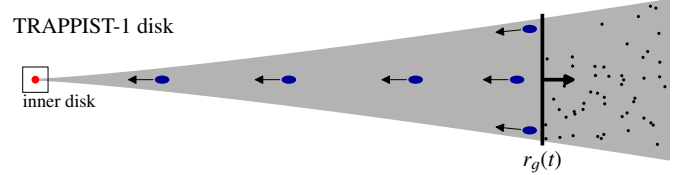


Fig. 1. The TRAPPIST-1 outer disk. Dust grains coagulate and drift inwards, resulting in a pebble front r_g that moves outwards with time. After $t = 10^5$ yr the pebble front will have reached 50 au. The box surrounding the star is then 1 au in size.

2012; Lambrechts & Johansen 2014; Krijt et al. 2016). For our standard disk parameters $\tau_p = 0.05$ at 0.1 au corresponds to a physical size of 4 cm. Interior to the iceline the size (and τ_p) will be smaller, because icy pebbles disintegrate.

2.2. The pebble mass flux

Most of the solids are located in the outer disk, initially in micron-size grains. Using an n - σ - Δv calculation, it follows that the collision timescales among grains is $t_{\text{coll}} \sim (Z_0 \Omega_K)^{-1}$, where Z_0 is the initial dust-to-gas ratio. Growth to pebble-size particles – large enough to start drifting – involves many binary collisions. Let $t_{\text{peb}} = \xi (Z_0 \Omega_K)^{-1}$, with $\xi \approx 10$ (Krijt et al. 2016), be the time needed before drifting pebbles appear. Equating $t = t_{\text{peb}}$ and solving for r we find the radius of the pebble front r_g where the particles reach their drifting size:

$$r_g = \left(\frac{GM_\star Z_0^2 t^2}{\xi^2} \right)^{1/3} = 50 \text{ au} \left(\frac{t}{10^5 \text{ yr}} \right)^{2/3}. \quad (4)$$

The advancing $r_g(t)$ generates pebbles at a rate $\dot{M}_p = 2\pi r_g \dot{r}_g Z_0 \Sigma_g(r_g)$ and results in a pebble-to-gas mass flux ratio of:

$$\mathcal{F}_{\text{p/g}} \equiv \frac{\dot{M}_p}{\dot{M}_g} = \frac{2M_{\text{disk}} Z_0^{5/3}}{3\dot{M}_g r_{\text{out}} \xi^{2/3}} \left(\frac{GM_\star}{t} \right)^{1/3} \approx 1.1 \left(\frac{t}{10^5 \text{ yr}} \right)^{-1/3} \quad (5)$$

(cf. Lambrechts & Johansen 2014). The pebble flux will disappear after the time t_{end} , when the pebble front hits the outer edge

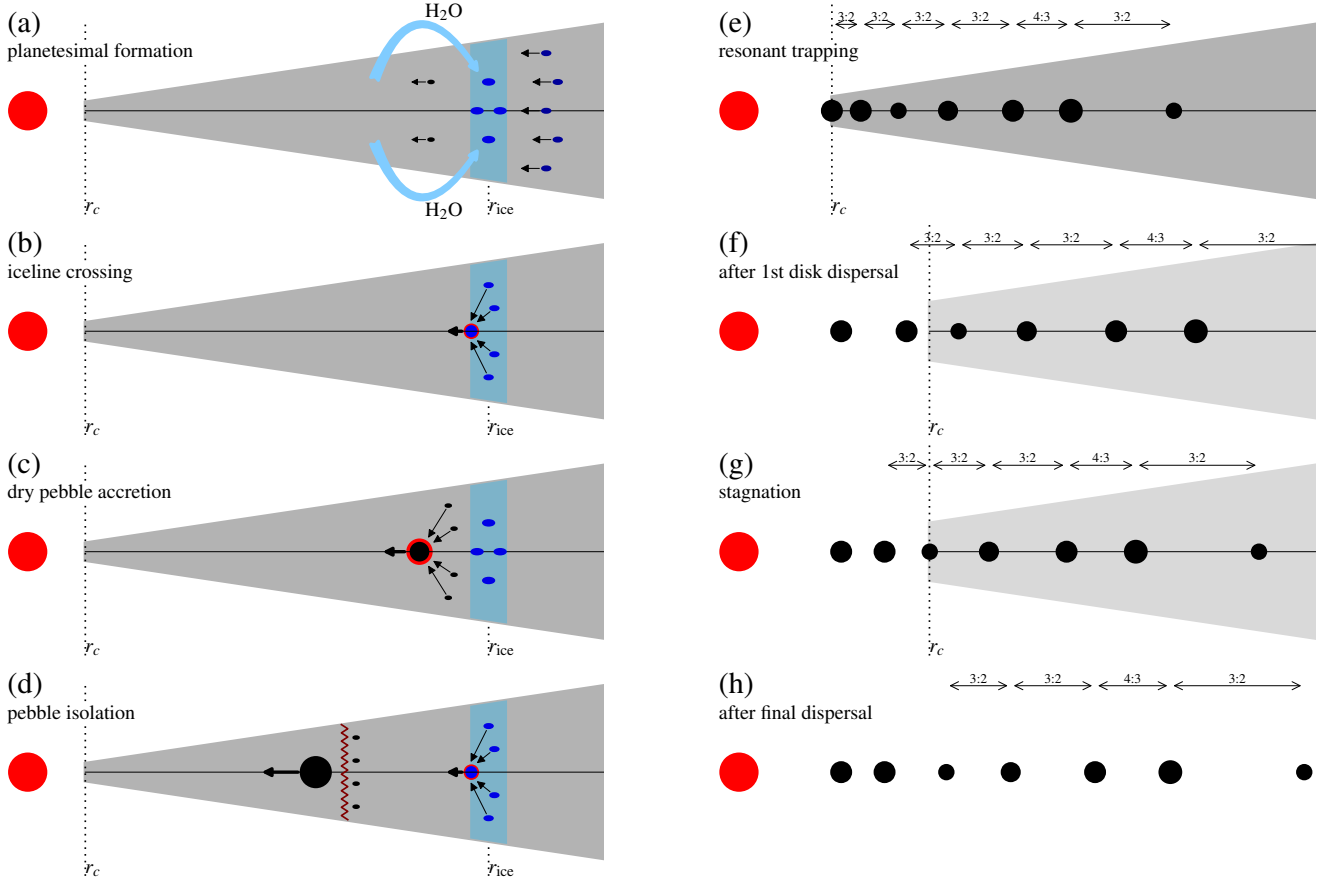


Fig. 2. Stages in the formation of the TRAPPIST-1 system. Panels shows the inner disk ($r \lesssim 0.1$ au): left panels describe the formation phases; right panels describe the disk dispersion and dynamical rearrangement. Stages are described in Sect. 3. Sizes and aspect ratios are not to scale, but relative distances are.

of the disk, $r_g = r_{\text{out}}$:

$$t_{\text{end}} = \frac{\xi}{Z_0} \sqrt{\frac{r_{\text{out}}^3}{GM_\star}} \approx 8 \times 10^5 \text{ yr} \quad (6)$$

3. Synopsis

In our scenario, the formation of the TRAPPIST-1 planets proceeds in two stages. In the first stage, planetary embryos assemble sequentially at the iceline, migrate inwards, and end up in resonance near the disk edge (panels a–d). The second stage concerns the dynamical re-arrangement, triggered by the disk dispersal, which moves the inner planets out of MMR (panels e–h).

In the first stage, our assumption is that planets form *sequentially*, not simultaneously. In our model we assume that the H_2O iceline is the location where the midplane solids-to-gas ratio exceeds unity, triggering streaming instabilities and spawning the formation of planetesimals. These planetesimals merge into planetary embryos, whose growth is aided by icy pebble accretion. Once its mass becomes sufficiently large, it migrates interior to the H_2O iceline by type I migration, where it continues to accrete (now dry) pebbles until it reaches the pebble isolation mass. After some time, a second embryo forms at the snowline, which follows a similar evolutionary path as its predecessor. Even though the inner planet’s growth could be reduced by its younger siblings’ appetite for pebbles, it always remains ahead in terms of mass. Planet migration stalls at the inner disk edge, where the planets are trapped in resonance.

3.1. Formation of planetesimals (a)

The first step is the concentration of pebble-size particles and their subsequent gravitational collapse into planetesimals. A prominent mechanism is the streaming instability, where particles clump into filaments because of the backreaction of the solids on the gas (Youdin & Goodman 2005). These filaments fragment and spawn planetesimals (Johansen et al. 2007). Recent work has demonstrated that streaming instabilities can be triggered for a broad range of stopping times (Yang et al. 2016); however a prerequisite is that the solids-to-gas ratio must be substantial (Johansen et al. 2009; Carrera et al. 2015; Yang et al. 2016). Since streaming instabilities arise by virtue of the backreaction of the solids on the gas, we seek volume solids-to-gas ratios $\rho_p/\rho_g \sim 1$.

However, the inside-out growth and drift of solids do not guarantee large solids-to-gas ratios (Birnstiel et al. 2010; Krijt et al. 2016; Sato et al. 2016). The midplane pebble-to-gas density ratio is only

$$\left(\frac{\rho_p}{\rho_g}\right)_{\text{midplane}} = \frac{\Sigma_p/H_p}{\Sigma_g/H_g} = \frac{3\mathcal{F}_{p/g}}{5} \sqrt{\frac{\alpha}{\tau_p}} \approx 0.08\mathcal{F}_{p/g} \quad (7)$$

where we used $\Sigma_g = \dot{M}_g/3\pi\nu$ with $\nu = \alpha h^2 r^2 \Omega$, $\Sigma_p = \mathcal{F}_{p/g} \dot{M}_g/2\pi r v_r$ with $v_r \approx 2\tau_p \eta v_K$, and a pebble-to-gas scaleheight of $H_p/H_g = \sqrt{\tau_p/\alpha}$ (Dubrulle et al. 1995). Therefore, the particle mass-loading is unlikely to approach unity.

To further enhance ρ_p/ρ_g we invoke the H_2O iceline, located at ≈ 0.1 au. Recently, we have demonstrated that enhancements

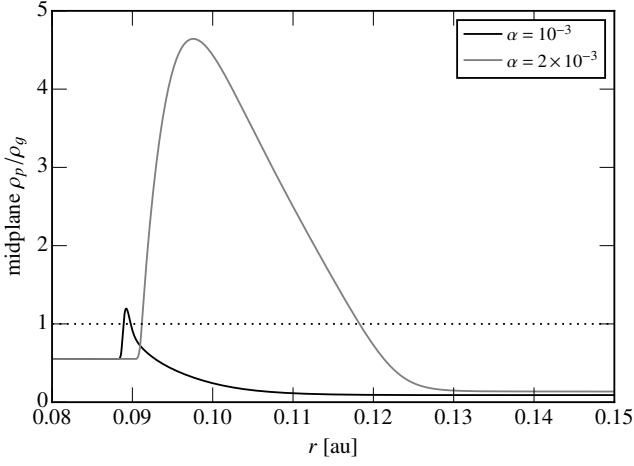


Fig. 3. Midplane solids-to-gas ratio for the many seed model design of Schoonenberg & Ormel (2017) with $\mathcal{F}_{p/g} = 1.1$ for $\alpha = 10^{-3}$ and 2×10^{-3} . The strong boost in solids-to-gas between the two runs arises from the backreaction of the solids on the gas, which reduces the radial drift of the particles resulting in a more significant pileup.

up to 10 can be attained (Schoonenberg & Ormel 2017).¹ Figure 3 presents the result of the Schoonenberg & Ormel (2017) ‘many-seed’ model for the iceline of TRAPPIST-1 disk. Due to diffusion, H_2O vapor is transported across the iceline where it condenses on the incoming pebbles, creating a distinct bump in the midplane pebble-to-gas ratio. For our standard parameters ($\alpha = 10^{-3}$) we find that ρ_p/ρ_g just exceeds unity, triggering the formation of planetesimals. The pebble-to-gas ratio increase as function of α for several reasons: (i) More H_2O vapor is being transported at larger α ; (ii) the base ρ_p/ρ_g (Eq. (7)) increases with α ; (iii) the backreaction of the solids on the gas, which start to become important at $\rho_p/\rho_g \sim 1$, reduces the particle drift, which strongly enhances the pileup effect. Finally, in Fig. 3 increasing α by a factor two happens to coincide with the Epstein-Stokes drag transition, which causes another jump (Schoonenberg & Ormel 2017).

On the other hand, for $\alpha < 10^{-3}$ pebble-to-gas ratios are likely to stay much below unity. However, disintegration of icy pebbles releases micron-size silicate grains, can create strong pileups just interior to r_{ice} (Saito & Sirono 2011). Ida & Guillot (2016) found that the midplane mass-loading of (silicate) grains is high enough to trigger direct gravitational instability, especially at low α . But even when particles re-coagulate their size is likely to be limited by collisional fragmentation or bouncing (e.g., Güttler et al. 2010), resulting in lower stopping times and dust-to-gas ratios high enough to trigger streaming instability (Banzatti et al. 2015; Drażkowska et al. 2016). In those cases, planets start out rocky and the phase described in the next subsection does not exist.

3.2. Migration interior to iceline (b)

We assume that a single, dominant planetary embryos emerges from the planetesimal-pebble mix. Its growth is indeed very

¹ Stevenson & Lunine (1988) and, more recently, Ros & Johansen (2013) already pointed to the H_2O iceline to trigger planetesimal formation and their subsequent growth. However, their models considered closed systems where either the particles or the gas was not removed from the system. In contrast, the steady-state model of Schoonenberg & Ormel (2017) features a constant inward mass flux of ice and gas.

rapid:

$$t_{\text{grow}} = \frac{M_{\text{pl}}}{\epsilon_{\text{PA}} \mathcal{F}_{p/g} \dot{M}_g} = \frac{q_{\text{pl}} M_{\star}}{\epsilon_{\text{PA}} \mathcal{F}_{p/g} \dot{M}_g} = \frac{8 \times 10^3 \text{ yr}}{\mathcal{F}_{p/g} \epsilon_{\text{PA}}} \left(\frac{q_{\text{pl}}}{10^{-5}} \right) \quad (8)$$

where $q_{\text{pl}} = M_{\text{pl}}/M_{\star}$ and ϵ_{PA} is the pebble accretion efficiency. We evaluate ϵ_{PA} in Sect. 3.3.

Planets migrate inwards at a rate r/t_I where t_I is the type I migration time:

$$t_I = \frac{h^2}{\gamma_I q_p q_{\text{gas}} \Omega_K} = \frac{3\pi\alpha h^4}{\gamma_I q_{\text{pl}} \dot{M}_g/M_{\star}} = 1.5 \times 10^5 \left(\frac{q_{\text{pl}}}{10^{-5}} \right)^{-1} \text{ yr} \quad (9)$$

where $q_{\text{gas}} = \Sigma_g r^2/M_{\star}$ and γ_I is of order unity (Tanaka et al. 2002; Kley & Nelson 2012). The planet crosses the iceline when $t_{\text{grow}} \approx \delta_{\text{ice}} t_I$ where $\delta_{\text{ice}} = \delta r_{\text{ice}}/r$ is the fractional width of the iceline. We therefore find that the embryo moves interior to the iceline at a mass:

$$M_{\text{cross}} = \sqrt{\frac{3\pi\alpha\delta_{\text{ice}}\mathcal{F}_{p/g}\epsilon_{\text{PA}}}{\gamma_I}} h^2 M_{\star} = 0.26 M_{\oplus} \sqrt{\mathcal{F}_{p/g}\epsilon_{\text{PA}}}. \quad (10)$$

With $\mathcal{F}_{p/g} = 1.1$ and $\epsilon_{\text{PA}} = 0.1$ (motivated in Sect. 3.3) this corresponds to a Mars-mass embryo of which $\approx 50\%$ is of icy composition. But the remainder of the accretion takes place in the interior region where pebbles are dry and the planet ends up predominantly rocky.

Note that the value of M_{cross} depends considerably on the viscosity parameter α . A larger α implies a lower gas density, suppressing migration, and a thicker ice-‘line’ (Schoonenberg & Ormel 2017), promoting a prolonged stay in the ice-rich region. For $\alpha \gtrsim 10^{-2}$ the crossover mass may well turn out to be similar to the pebble isolation mass (see below), such that the planet will have a high H_2O content.

3.3. Efficient pebble accretion (b,c)

Planetesimals formed by streaming instability can have sizes up to ~ 100 km (Simon et al. 2016; Schäfer et al. 2017). These planetesimals will accrete the pebbles that are drifting from the outer disk, in so-called settling interactions (Ormel & Klahr 2010). This mechanism, more popularly known as pebble accretion (Lambrechts & Johansen 2012), is particularly attractive in case of TRAPPIST-1, because it is highly efficient – a large fraction of the pebbles are accreted.

First, consider pebble accretion exterior to the iceline. We assume that pebble accretion operates in the planar (2D) mode, which is appropriate for low-to-moderate α . Accretion of pebbles in the planar mode amounts to a rate of (Ida et al. 2016; Ormel 2017):

$$\dot{M}_{\text{pl}} \sim 2R_{\text{Hill}}^2 \Omega_K \tau_p^{2/3} \Sigma_p, \quad (11)$$

where $R_{\text{Hill}} = r(q_{\text{pl}}/3)^{1/3}$ is the Hill radius. Since the pebble flux is $(2\pi r)v_r \Sigma_p$, pebbles are accreted at an efficiency of

$$\epsilon_{\text{PA}} \sim \frac{2}{5 \cdot 3^{2/3} \pi \tau_p^{1/3}} \left(\frac{q_{\text{pl}}}{h^3} \right)^{2/3} = 0.1 \left(\frac{q_{\text{pl}}}{10^{-5}} \right)^{2/3}, \quad (12)$$

where we inserted $v_r \approx \frac{5}{2} h^2 \tau_p \Omega_K r$ (Sect. 2). In a more precise, N-body calculation (Liu & Ormel 2017, in prep) we find $\epsilon_{\text{PA}} = 0.25$ for $q_{\text{pl}} = 10^{-5}$. Compared to solar-type stars, pebble accretion for the TRAPPIST-1 disk is particularly efficient because the disk is thin (pebbles are accreted in the 2D limit) and Hill radii are larger due to the low stellar mass.

Next, consider pebble accretion interior to the iceline. Although the grains liberated by sublimating icy pebbles are likely to have re-coagulated, their sizes are much lower because of the silicate fragmentation threshold. Therefore, $\tau_s \ll \tau_p$ ('s' referring to silicate pebbles) and pebble accretion operates in the 3D limit (Ida et al. 2016; Ormel 2017):

$$\dot{M}_{\text{pl-3D}} \sim 6\pi R_{\text{Hill}}^3 \tau_s \Omega \rho_s \quad (13)$$

where ρ_s is the midplane density of silicate pebbles. In the limit, where silicate pebbles are distributed over the entire gas scale-height, $\rho_s = \Sigma_s/2h$ with Σ_s the silicate surface density interior to the iceline, we obtain an efficiency of

$$\epsilon_{\text{PA-3D}} = \frac{\dot{M}_{\text{pl-3D}}}{(2\pi r)(2\eta\tau_s r \Omega) \Sigma_s} \sim \frac{1}{5} \frac{q_{\text{pl}}}{h^3} = 0.07 \left(\frac{q_{\text{pl}}}{10^{-5}} \right). \quad (14)$$

This estimate is conservative: settling increases efficiencies by a factor $\sqrt{\tau_s/\alpha}$ and numerically-obtained rates are typically higher by a factor two. Hence, growth remains rapid; from Eq. (8) we obtain a growth time of $t_{\text{grow}} \sim 10^5 \text{ yr} / \mathcal{F}_{\text{s/g}}$, where $\mathcal{F}_{\text{s/g}}$ is now the silicate-to-gas mass flux ratio.

Our results differ in two aspects from Morbidelli et al. (2015), who also calculated pebble accretion interior and exterior to the iceline. In Morbidelli et al. (2015) embryos are kept at fixed locations (no migration) and the outer embryo, growing faster, was seen to ultimately starve the inner from pebbles. In our scenario there is no true competition, due to the aforementioned sequential growth and migration. The second difference is that q_{pl}/h^3 , which enters the efficiency expressions at different powers (Eq. (12) vs Eq. (14)), is much larger in TRAPPIST-1. When embryos cross the iceline we have $q_{\text{pl}}/h^3 \sim 0.1$, whereas Morbidelli et al. (2015) starts from $q_{\text{pl}}/h^3 \sim 10^{-4}$. Therefore, in Morbidelli et al. (2015) the 2D-rate (exterior to the iceline) is much larger than the 3D-rates (interior), whereas in the case of TRAPPIST-1 there is no significant difference.

3.4. Pebble isolation (d)

Pebble accretion terminates when the gravitational feedback of the planet on the disk becomes important. At such pressure maxima pebbles stop drifting. Essentially, pebble isolation describes the onset of gap opening. While the pebble isolation mass for disks around solar-type stars at 5 au is $\approx 20 M_{\oplus}$ (Lambrechts et al. 2014), it will be much smaller at the iceline of the TRAPPIST-1 disk. A necessary condition for gap opening is that the Hill radius exceed the disk scaleheight, $q_{\text{pl}} = M_{\text{pl}}/M_{\star} > h^3$ (Lin & Papaloizou 1993); therefore:

$$M_{\text{p,iso}} \sim h^3 M_{\star} = 0.72 M_{\oplus}. \quad (15)$$

These arguments have motivated us to adopt $h \approx 0.03$, but this choice is not unreasonable. The fact that Earth-mass planets naturally emerge from the pebble-driven growth scenario is a distinctive feature of the model.

After the inner-most planet first reaches the pebble isolation mass, which from the above reasoning occurs after $\sim 2 \times 10^5 \text{ yr}$, silicates pebbles no longer accrete on TRAPPIST-1. From that point on, the entire silicates mass reservoir – except those grains so tiny that they follow the gas (Zhu et al. 2012) – are available to make planets, resulting in a high global formation efficiency. Before isolation has been reached, the inner-most planet loses $(1 - \epsilon_{\text{PA-3D}})/\epsilon_{\text{PA-3D}}$ pebbles for every silicate pebble it accretes. Evaluating this number at the final mass of the planet (1 Earth mass or $q_{\text{pl}} = 3.7 \times 10^{-5}$) we obtain that ~ 3 Earth mass

in silicates are lost. Our mechanism therefore efficiently turns solids into planets. An efficient mechanism is indeed necessary, because the initial disk contains only 11 Earth mass in rocky materials (Sect. 2).

3.5. Migration and resonance trapping (d)–(e)

On timescales $\sim t_I$ planets Type-I migrate to the disk edge (r_c). We assume here, for simplicity, that the migration is always inwards – *i.e.*, no special thermodynamical effects that could reverse the migration sign (Paardekooper et al. 2011; Benítez-Llambay et al. 2015). The processes illustrated in Fig. 2a–c then repeat until a convoy of seven planets is established.

Convergent migration of planets naturally results in resonant trapping (Terquem & Papaloizou 2007). For our disk model planets are likely to be trapped in the 2:1 MMR. According to Ogiwara & Kobayashi (2013) the condition to avoid trapping in the 2:1 resonance reads²:

$$t_I < t_{\text{a,crit}} \approx 4 \times 10^3 \text{ yr} \left(\frac{r}{0.1 \text{ au}} \right)^{3/2} \quad (16)$$

i.e., we have that t_I (Eq. (9)) is too long by a factor ≈ 10 at 0.1 au and the disparity only increases with lower r . However, most planets are observed near the 3:2 MMR. A quantitative model to explain the settling into the 3:2 MMR resonance is beyond the scope of this Paper but we offer several ideas for further investigation:

- The TRAPPIST-1 planets will form a resonant convoy, where all outer planets ‘push’ on the inner-most ones, effectively increasing γ_I and decreasing the migration timescale (McNeil et al. 2005). For low- α disk ($\alpha = 10^{-4}$) gas densities are also larger by a factor 10 and we can expect planets to be moved across the 2:1.
- Stochastic forces driven by density fluctuations in a disk from *e.g.*, MRI-turbulence (Okuzumi & Ormel 2013) can move planets across resonances (Paardekooper et al. 2013). Similarly, the disk accretion rate \dot{M}_g , assumed constant here, is likely to vary in time (Hartmann 2009). At intervals where \dot{M} peaks the condition $t_I < t_{\text{a,crit}}$ can be fulfilled.
- Period ratios may already be interior to 2:1 from the point where the outer planet crosses the iceline. Indeed, since $t_{\text{grow}} \leq t_I$ it is plausible to assume that the inner planet will not have migrated to the cavity radius before the next planet crosses the iceline. To ensure that the interior planet resides between the 3:2 and 2:1 resonant location at the time of iceline crossing requires a certain level of fine-tuning, however.

Investigating each of these scenarios requires a dedicated numerical simulations. In the following, we just assume that the planets end up in MMR resonance, as shown in Fig. 2e.

3.6. Disk dispersal and rebound (f)–(h)

Planet pairs b/c and c/d are presently not near the 3:2 MMR. Several mechanisms have been proposed to move planets out of resonance, *e.g.*, damping by stellar tides (Lithwick & Wu 2012) or giant impacts (Ogiwara et al. 2015). Here we consider *magnetospheric rebound* (Liu et al. 2017), which relies on the outward movement of the stellar magnetospheric cavity r_c during disk dispersal. In principle, the inner-most planet at $r = r_c$ is tightly coupled to the disk by strong one-sided torques (Liu et al. 2017).

² Here, we evaluated Equation (4) of Ogiwara & Kobayashi 2013 for $M_{\text{pl}} = M_{\oplus}$ and $M_{\star} = 0.08 M_{\odot}$.

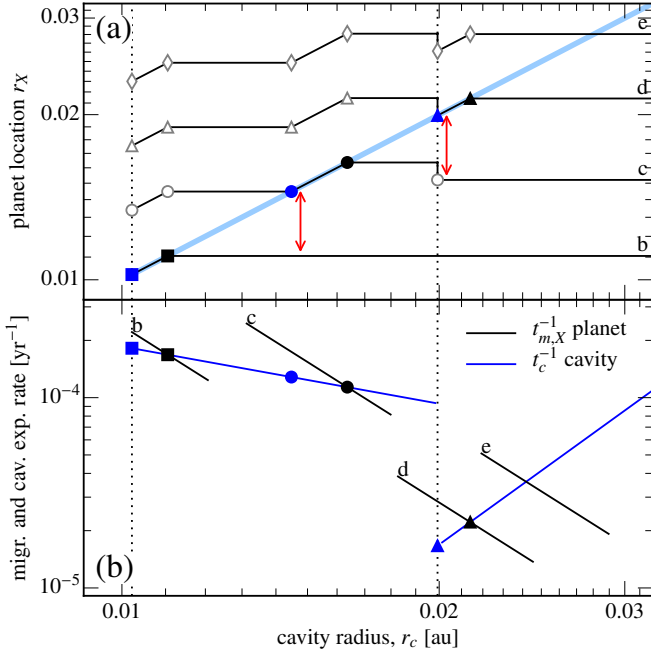


Fig. 4. Resonance escape. *Bottom:* one-sided migration rates $t_{m,X}^{-1}$ as function of cavity radius r_c for planet X (black lines; labeled) and expansion rate of the magnetospheric cavity t_c^{-1} (blue lines). The form $t_c(r_c)$ is chosen to fit the orbital configuration of the TRAPPIST-1 system. The jump in t_c at $r_c = 0.02$ au indicates that \dot{M}_g and $r_c(t)$ are temporarily constant. Blue symbols denote a planet that couples to (move synchronously with) the cavity radius. Black symbols denote the point of decoupling (the planet falls into the cavity). *Top:* the location of the planets corresponding to $r_c(t)$. Red arrows indicate the point where the 3:2 resonance is broken, because of divergent migration.

It therefore tends to follow the expanding r_c . But when the cavity expansion is too rapid – *i.e.*, when the expansion rate is higher than the planet migration rate – the planet decouples and falls in the magnetospheric cavity.

We have tuned the detailed behavior of $r_c(t)$ (or, equivalently, $\dot{M}(t)$ by Eq. (3)) in order to retrieve the orbital parameters of TRAPPIST-1. In Fig. 4a we plot the positions of planets b–e as function of the (expanding) cavity radius r_c (for clarity we omit planets f, g, and h). Note that r_c is used as a proxy for time. In Fig. 4b we plot the rate at which the cavity expands ($t_c^{-1} = \dot{r}_c/r_c$, blue curve) and the maximum one-sided planet migration rates, $t_{m,X}^{-1}$, for the planets (b, c, d, or e):

$$t_{m,X}^{-1} = 2C_{\text{hs}}q_{\text{gas}} \left(\frac{q_{\text{pl}}}{h^3} \right)^{1/2} \Omega_K \propto C_X \left(\frac{r_c}{r_{c0}} \right)^{-3.5}. \quad (17)$$

(Liu et al. 2017). The key point is that for any planet $t_{m,X}^{-1} \propto \dot{M}_g \propto r_c^{-3.5}$ (see Eq. (3)) and that it depends, through C_X , on the planet properties: more massive planets tend to have larger C_X and C_X also decreases with the number of planets in a resonance chain. Here we take $t_c \sim 10^4$ yr (with a dependence on r_c as in Fig. 2b) and $C_X = \{1.5, 4, 2., 5\}$.

Our model features a two-stage disk dispersal. First, r_c doubles from 0.01 to 0.02 au, where it temporarily stalls (Fig. 2f). Planet b decouples relative quickly from the expanding cavity front, whereas the more massive planet c couples longer to r_c due to its larger C_X . The 3:2 resonance between planets b and c is broken because of divergent migration just after the coupling of c to the cavity radius.

During the time when r_c pauses at 0.02 au, the accretion rate \dot{M}_g is constant. We assume that this phase takes long enough for planet d to migrate inward, such that it now coincides with the cavity radius (Fig. 2g). Planets c, e and f–h (not shown in Fig. 2) follow suit as they are still part of the resonance chain.

During the second dispersal phase planet d only briefly couples to the expanding r_c , but enough to escape resonance with c. Afterwards, the expansion proceeds too rapid for planets to couple. For example, at the point where r_c meets planet e ($r_c \approx 0.028$ au) the one-sided migration rate is at least a factor three less than \dot{r}_c . Therefore, e and the other outer planets stay in resonance.

In the above discussion, we have referred to ‘resonance’ as exact commensurability (nominal resonance). However, planets moving away from exact commensurability can maintain librating resonant angles; Batygin & Morbidelli (2013) found that dissipative divergence in this way keeps planet in resonance in the dynamical sense. Luger et al. (2017) have shown that the TRAPPIST-1 planets form a complex chain of three-body resonances.³ Long-term dynamical stability would be greatly promoted when the initial libration width of the resonant angles is small (Tamayo et al. 2017) or when stellar tides play a role (Paloizou 2015).

4. Closing remarks

In this Paper we have outlined a new framework to understand the formation of planetary systems around very low mass stars. With some modest tuning, we have succeeded in obtaining a system whose architecture reflects that of TRAPPIST-1 (Fig. 2h). Its most radical idea is that planets assemble at a specific location – the H₂O iceline. This contrasts classical models, where planets form locally, as well as population synthesis models, which do account for migration but do not (yet) provide a physical model for the initial position of planetary embryos. Our scenario is more complete, as we provide a physical model where planetary embryos (first) form.

Nevertheless, several parts of the proposed scenario require further investigation. We already mentioned the difficulty of avoiding the planets to get trapped in the 2:1 MMR, because of the rather low disk mass (Sect. 3.5). Another key assumption of our scenario is that one embryo-at-a-time emerges from the iceline. Simultaneous formation of multiple embryos could result in an excited system of small embryos, suppressing growth (Kretke & Levison 2014, but see Levison et al. 2015). Because of the short dynamical timescales, it seems viable that bodies quickly coalesce, but this complex issue – how does streaming instability operate in the presence of planetary embryo’s? – warrants further investigation.

A prominent feature of our model is that planets mature in gas-rich disks; there is no need for a post-disk giant impact phase. Therefore, the TRAPPIST-1 planets could have accreted primordial H/He atmospheres, for which there is, presently, no indication of (de Wit et al. 2016). However, planets close to their host star receive high doses of UV and X-ray fluxes (Stelzer et al. 2013; Bourrier et al. 2017), stripping their atmospheres away efficiently (Lopez et al. 2012). Composition-wise, the inferred densities of 3–6 g cm $^{-3}$ (Gillon et al. 2017) rule out that these planets are entirely composed of H₂O. But given the error bars on the mass, planets are consistent with large ($\sim 10\%$) H₂O

³ From timing analysis it is much easier to identify a three-body resonance, for which only the mean longitude are important, rather than two-body resonance, which require the arguments of periapses.

fractions – in particular planet f – making these planets ‘water worlds’, even if many (Earth) oceans of H_2O were lost (Bolmont et al. 2017). In the context of our model the maximum H_2O fraction is $\approx 50\%$ when the planets reach their isolation mass at the H_2O iceline.

The model that we outlined here can also be applied to compact systems around higher mass stars. Early-type M-stars exhibit a large concentration of planets at close distances (Dressing & Charbonneau 2015). In addition, *Kepler* has found many compact systems of super-Earth planets around solar-mass stars (Petigura et al. 2013). In our model the typical planet mass scale is $\sim h^3 M_\star$ (Eq. (15)), which would correspond to $\sim 10 M_\oplus$ for solar-mass stars (still assuming $h = 0.03$). The observation that fewer large (Neptune-like) planets are found around M-stars as compared to FGK-stars (Mulders et al. 2015) therefore agrees with one of the pillars of our scenario: that the upper mass limit of rocky planets is set by the pebble isolation mass.

The key characteristic of our model is that close-in planets formed by tapping the pebble flux that originated from large distances (~ 10 – 100 au). This assumes that pebbles drifted unimpededly: the disk has to be smooth. Also, we have argued that the natural location to form a planet rapidly is the H_2O iceline, which, for solar-type stars is located at ~ 2 – 3 au. When growth at the iceline proceeds rapidly, a $\sim 10 M_\oplus$ core forms a large, pre-planetary H/He-atmospheres, which can collapse into a giant planet upon reaching the critical core mass – and a H_2O -enriched atmosphere would greatly accelerate this process (Venturini et al. 2015). When indeed a giant planet would form *rapidly* at the snowline, it terminates the pebble flux to the inner disk, starving it from planet-building material and rendering it dry (Morbidelli et al. 2016). Hence, we expect a dichotomy: when giant planet formation fails, pebbles can drift across the iceline to aid the growth of super-Earths and mini-Neptunes. Conversely, when a giant planet forms at the iceline we expect a dearth of planetary building blocks close in. Therefore, the close-in super-Earth population found by *Kepler* and the cold Jupiter populations found chiefly by radial velocity surveys should be anti-correlated⁴ – a prediction that could be tested with future exoplanet surveys.

Acknowledgements. We thank Anders Johansen, Allona Vazan, Andrius Popovas, Carsten Dominik, Jean-Michel Désert, Samaya Nisanke, and Sebastiaan Krijt for useful discussions and the referee for a critical report that sharpened the presentation. The authors are supported by the Netherlands Organization for Scientific Research (NWO; VIDI project 639.042.422).

References

Banzatti, A., Pinilla, P., Ricci, L., et al. 2015, *ApJ*, 815, L15
 Batygin, K. & Morbidelli, A. 2013, *AJ*, 145, 1
 Benítez-Llambay, P., Masset, F., Koenigsberger, G., & Szulágyi, J. 2015, *Nature*, 520, 63
 Birnstiel, T., Andrews, S. M., & Ercolano, B. 2012, *A&A*, 544, A79
 Birnstiel, T., Dullemond, C. P., & Brauer, F. 2010, *A&A*, 513, A79
 Bolmont, E., Selsis, F., Owen, J. E., et al. 2017, *MNRAS*, 464, 3728
 Bourrier, V., Ehrenreich, D., Wheatley, P. J., et al. 2017, *A&A*, 599, L3
 Carrera, D., Johansen, A., & Davies, M. B. 2015, *A&A*, 579, A43
 de Wit, J., Wakeford, H. R., Gillon, M., et al. 2016, *Nature*, 537, 69
 Drążkowska, J., Alibert, Y., & Moore, B. 2016, *A&A*, 594, A105
 Dressing, C. D. & Charbonneau, D. 2015, *ApJ*, 807, 45
 Dubrulle, B., Morfill, G., & Sterzik, M. 1995, *Icarus*, 114, 237
 Frank, J., King, A., & Raine, D. 1992, *Accretion power in astrophysics*.
 Gillon, M., Jehin, E., Lederer, S. M., et al. 2016, *Nature*, 533, 221
 Gillon, M., Triaud, A. H. M. J., Demory, B.-O., et al. 2017, *Nature*, 542, 456

Güttler, C., Blum, J., Zsom, A., Ormel, C. W., & Dullemond, C. P. 2010, *A&A*, 513, A56
 Hansen, B. M. S. & Murray, N. 2012, *ApJ*, 751, 158
 Hartmann, L. 2009, *Accretion Processes in Star Formation: Second Edition* (Cambridge University Press)
 Ida, S. & Guillot, T. 2016, *A&A*, 596, L3
 Ida, S., Guillot, T., & Morbidelli, A. 2016, *A&A*, 591, A72
 Izidoro, A., Morbidelli, A., Raymond, S. N., Hersant, F., & Pierens, A. 2015, *A&A*, 582, A99
 Johansen, A., Oishi, J. S., Low, M., et al. 2007, *Nature*, 448, 1022
 Johansen, A., Youdin, A., & Mac Low, M. 2009, *ApJ*, 704, L75
 Kley, W. & Nelson, R. P. 2012, *ARA&A*, 50, 211
 Kretke, K. A. & Levison, H. F. 2014, *AJ*, 148, 109
 Krijt, S., Ormel, C. W., Dominik, C., & Tielens, A. G. G. M. 2016, *A&A*, 586, A20
 Lambrechts, M. & Johansen, A. 2012, *A&A*, 544, A32
 Lambrechts, M. & Johansen, A. 2014, *A&A*, 572, A107
 Lambrechts, M., Johansen, A., & Morbidelli, A. 2014, *A&A*, 572, A35
 Lee, M. H. & Peale, S. J. 2002, *ApJ*, 567, 596
 Levison, H. F., Kretke, K. A., & Duncan, M. J. 2015, *Nature*, 524, 322
 Lin, D. N. C. & Papaloizou, J. C. B. 1993, in *Protostars and Planets III*, ed. E. H. Levy & J. I. Lunine, 749–835
 Lithwick, Y. & Wu, Y. 2012, *ApJ*, 756, L11
 Liu, B. & Ormel, C. W. 2017, in prep
 Liu, B., Ormel, C. W., & Lin, D. N. C. 2017, *ArXiv e-prints*:1702.02059
 Lodders, K. 2003, *ApJ*, 591, 1220
 Lopez, E. D., Fortney, J. J., & Miller, N. 2012, *ApJ*, 761, 59
 Luger, R., Sestovic, M., Kruse, E., et al. 2017, *ArXiv e-prints*:1703.04166
 Lynden-Bell, D. & Pringle, J. E. 1974, *MNRAS*, 168, 603
 Manara, C. F., Testi, L., Natta, A., & Alcalá, J. M. 2015, *A&A*, 579, A66
 McNeil, D., Duncan, M., & Levison, H. F. 2005, *AJ*, 130, 2884
 Morbidelli, A., Bitsch, B., Crida, A., et al. 2016, *Icarus*, 267, 368
 Morbidelli, A., Lambrechts, M., Jacobson, S., & Bitsch, B. 2015, *Icarus*, 258, 418
 Mulders, G. D. & Dominik, C. 2012, *A&A*, 539, A9
 Mulders, G. D., Pascucci, I., & Apai, D. 2015, *ApJ*, 814, 130
 Nakagawa, Y., Sekiya, M., & Hayashi, C. 1986, *Icarus*, 67, 375
 Ogihara, M. & Kobayashi, H. 2013, *ApJ*, 775, 34
 Ogihara, M., Morbidelli, A., & Guillot, T. 2015, *A&A*, 578, A36
 Okuzumi, S. & Ormel, C. W. 2013, *ApJ*, 771, 43
 Ormel, C. W. 2017, in *Formation, Evolution, and Dynamics of Young Solar Systems*, ed. Gressel, O. & Pessah, M., *Proceedings of the Sant Cugat Forum on Astrophysics* (Springer)
 Ormel, C. W. & Klahr, H. H. 2010, *A&A*, 520, A43
 Paardekooper, S.-J., Baruteau, C., & Kley, W. 2011, *MNRAS*, 410, 293
 Paardekooper, S.-J., Rein, H., & Kley, W. 2013, *MNRAS*, 434, 3018
 Papaloizou, J. C. B. 2015, *International Journal of Astrobiology*, 14, 291
 Pérez, L. M., Chandler, C. J., Isella, A., et al. 2015, *ApJ*, 813, 41
 Petigura, E. A., Marcy, G. W., & Howard, A. W. 2013, *ApJ*, 770, 69
 Rafikov, R. R. & De Colle, F. 2006, *ApJ*, 646, 275
 Reiners, A., Basri, G., & Christensen, U. R. 2009, *ApJ*, 697, 373
 Ricci, L., Testi, L., Natta, A., Scholz, A., & de Gregorio-Monsalvo, I. 2012, *ApJ*, 761, L20
 Ros, K. & Johansen, A. 2013, *A&A*, 552, A137
 Saito, E. & Sirono, S.-i. 2011, *ApJ*, 728, 20
 Sato, T., Okuzumi, S., & Ida, S. 2016, *A&A*, 589, A15
 Schäfer, U., Yang, C.-C., & Johansen, A. 2017, *A&A*, 597, A69
 Schoonenberg, D. & Ormel, C. W. 2017, *ArXiv e-prints*:1702.02151
 Simon, J. B., Armitage, P. J., Li, R., & Youdin, A. N. 2016, *ApJ*, 822, 55
 Stelzer, B., Marino, A., Micela, G., López-Santiago, J., & Liefke, C. 2013, *MNRAS*, 431, 2063
 Stevenson, D. J. & Lunine, J. I. 1988, *Icarus*, 75, 146
 Tamayo, D., Rein, H., Petrovich, C., & Murray, N. 2017, *ArXiv e-prints*:1704.02957
 Tanaka, H., Takeuchi, T., & Ward, W. R. 2002, *ApJ*, 565, 1257
 Terquem, C. & Papaloizou, J. C. B. 2007, *ApJ*, 654, 1110
 Testi, L., Birnstiel, T., Ricci, L., et al. 2014, *Protostars and Planets VI*, 339
 Venturini, J., Alibert, Y., Benz, W., & Ikoma, M. 2015, *A&A*, 576, A114
 Weidenschilling, S. J. 1977, *MNRAS*, 180, 57
 Yang, C.-C., Johansen, A., & Carrera, D. 2016, *ArXiv e-prints*:1611.07014
 Youdin, A. N. & Goodman, J. 2005, *ApJ*, 620, 459
 Zhu, Z., Nelson, R. P., Dong, R., Espaillat, C., & Hartmann, L. 2012, *ApJ*, 755, 6

⁴ Izidoro et al. (2015) arrived at the same prediction, but from a different context. In their scenario, giant planets block the migration of super-Earths and mini-Neptunes, which formed even further in the outer disk.